ACS APPLIED MATERIALS & INTERFACES

www.acsami.org

Research Article

Ultrastable 3D Heterogeneous Integration via N-Heterocyclic Carbene Self-Assembled Nanolayers

Jinhyoung Lee, Gunhoo Woo, Gyuyoung Lee, Jongyeong Jeon, Seunghwan Lee, Ziyang Wang, Hyelim Shin, Gil-Woo Lee, Yeon-Ji Kim, Do-Hyun Lee, Min-Jae Kim, Eungchul Kim, Hyunho Seok, Jinill Cho, Boseok Kang, You-Shin No, Won-Jun Jang, and Taesung Kim*

Cite This: https://doi.org/10.1021/acsami.4c04665

Read Online

ACCESS | Metrics & More | Article Recommendations | Supporting Information

ABSTRACT: The commercialization of 3D heterogeneous integration through hybrid bonding has accelerated, and accordingly, Cu−polymer bonding has gained significant attention as a means of overcoming the limitations of conventional Cu−SiO_2 hybrid bonding, offering high compatibility with other fabrication processes. Polymers offer robust bonding strength and a low dielectric constant, enabling high-speed signal transmission with high reliability, but suffer from low thermomechanical stability. Thermomechanical stability of polymers was not achieved previously because of thermal degradation and unstable anchoring. To overcome these limitations, wafer-scale Cu−polymer bonding via N-heterocyclic carbene (NHC) nanolayers was presented for 3D heterogeneous integration, affording ultrastable packing density, crystallinity, and thermal properties. NHC nanolayers were deposited on copper electrodes via electrochemical deposition, and wafer-scale 3D heterogeneous integration was achieved by adhesive bonding at 170 °C for 1 min. Ultrastable conductivity and thermomechanical properties were observed by the spatial mapping of conductivity, work function, and force−distance curves. With regard to the characterization of NHC nanolayers, low-temperature bonding, robust corrosion inhibition, enhanced electrical conductivity, back-end-of-line process compatibility, and fabrication process reduction, NHC Cu/polymer bonding provides versatile advances in 3D heterogeneous integration, indicating that NHC Cu/polymer bonding can be utilized as a platform for future 3D vertical chip architectures.

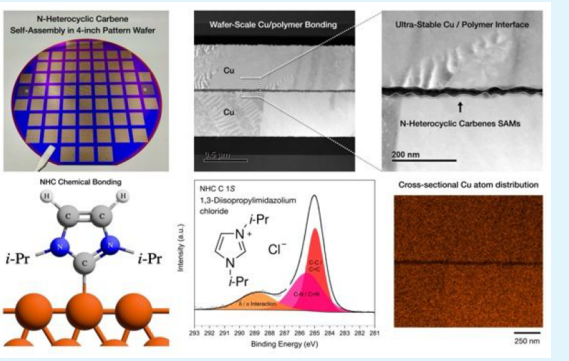

KEYWORDS: *N-heterocyclic carbenes, Cu/polymer bonding, self-assembly, 3D heterogeneous integration, charge transfer*

1. INTRODUCTION

The semiconductor industry has focused on scaling down the transistor size and line width to achieve higher performance, smaller form factors, and lower manufacturing costs. However, the limits of Moore's law have recently been reached as the scaling of transistor devices has been pushed to its physical limits. Despite extensive efforts to maintain Moore's law, including device miniaturization reduction, such as in EUV[1] and ultrathin 2D materials,[2] there are many practical limitations to implementing these technologies. As it becomes more difficult to scale down transistors within the 2D in-plane space, 3D vertical integration of chips is gaining tremendous attention for overcoming the physical limitations of semiconductor devices. Vertical 3D structures[3] are conventionally prepared via two integration methods: 3D monolithic integration (MI) and 3D heterogeneous integration (HI). In various studies on 3D monolithic integration, single-crystal films were grown based on van der Waals epitaxy,[4,5] remote epitaxy,[6] and pinhole epitaxy;[7] however, monolithic growth is not easily commercialized owing to difficulties in meeting fabrication capability and cost requirements. Conversely, 3D HI offers speed, cost reduction, and process simplification by chemical mechanical planarization (CMP)[8] of the metal surface without dishing and erosion, followed by bonding at high temperature and pressure to easily integrate different components; therefore, there is a tremendous demand for wafer-scale 3D HI.[9]

While the Cu−SiO_2 bonding,[10] a widely used hybrid bonding process for HI, has been studied and developed over the past decades, Cu−SiO_2 bonding has several critical limitations.[11] The first limitation of Cu−SiO_2 bonding is the heterogeneity of the coefficient of thermal expansion (CTE) of Cu−SiO_2.[12,13] Because direct bond interconnect (DBI) bonding is typically performed at high temperatures (approx-

Received: March 21, 2024
Revised: June 7, 2024
Accepted: June 11, 2024

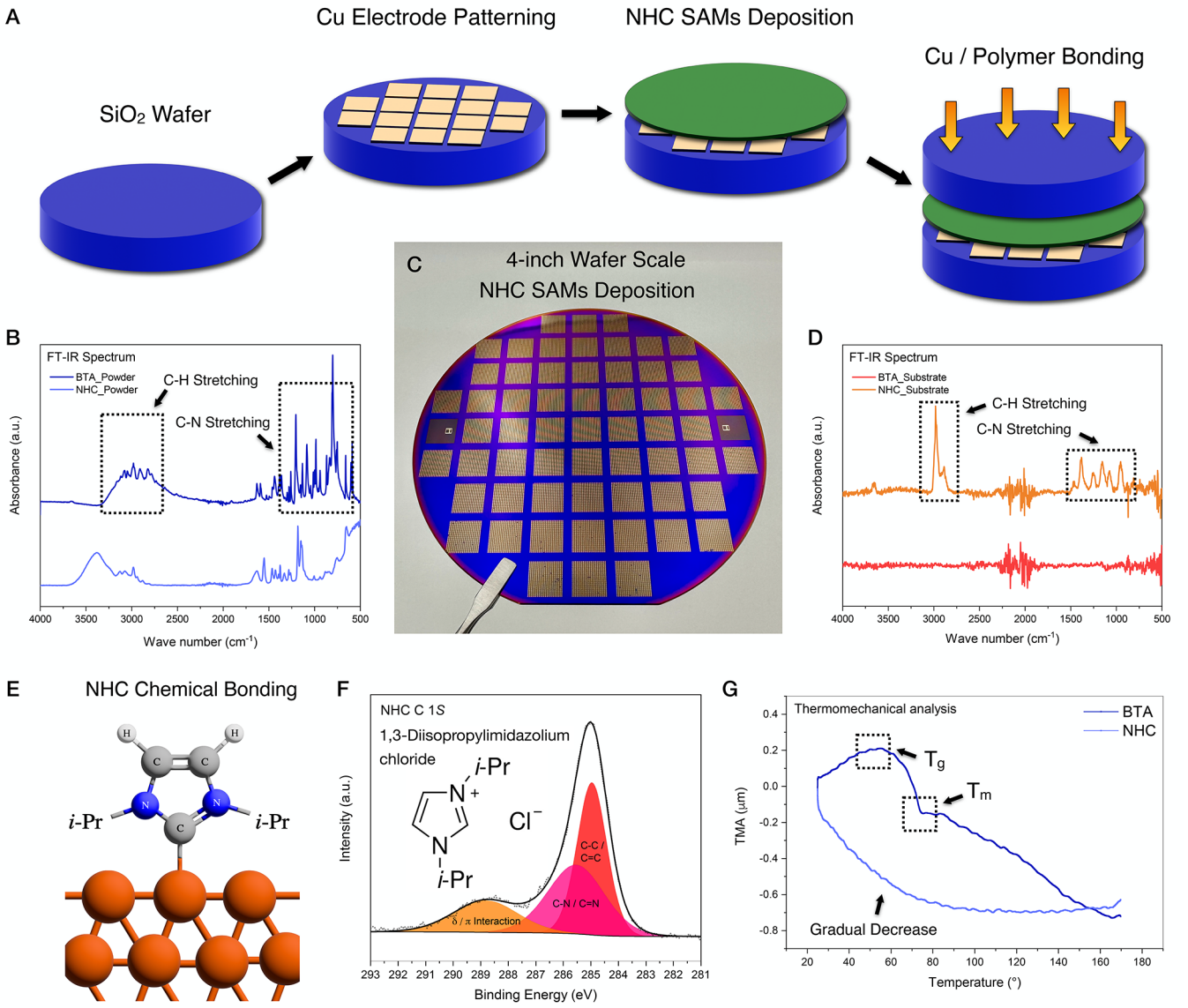

Figure 1. Wafer-scale Cu/polymer bonding via NHC nanolayers. (A) Schematic of experimental process for Cu/polymer bonding with NHC nanolayers. (B) FT-IR spectra of NHC and BTA in powder state. (C) Photograph of electrochemically deposited NHC nanolayers on 4 in. wafer-scale Cu electrode. (D) FT-IR spectra of NHC and BTA in passivationlayer state. (E) Atomic-scale chemical bonding structure of NHC self-assembled on Cu (111) surfaces, which anchored with Cu−carbene covalent bonds. (F) XPS C 1s spectra of NHC nanolayers, which clarify the formation of covalent Cu−C bonds, enabling charge transfer at the metal−molecule interfaces. (G) Thermomechanical analysis of organic passivation layers, showing heterogeneity of thermomechanical displacement between BTA and NHC.

imately 250 °C), the difference in the CTE of the two materials can lead to mechanical deformation during the DBI bonding process at high temperatures.[14] This can induce the formation of microvoids, misalignment at the bonding interface, and reduced reliability in heterogeneous integration. Moreover, the bonding strength of SiO_2 is insufficient for reliable hybrid bonding.[12,13] The low chemical bonding strength can reduce the packaging yield and limit the applications of 3D functional chips. Owing to various critical limitations, reliable 3D packaging is not achievable for Cu−SiO_2 bonding. Therefore, Cu−polymer bonding is gaining attention as a next-generation bonding method[15,16] for achieving low-*K* properties,[17] Cu migration resistance,[18] and high warpage tolerance.[19] However, the thermal stability of polymers is extremely low compared to that of other materials.[20,21]

Thus, Cu−polymer bonding cannot be commercialized for wafer-scale production due to their critical limitations.[22] The polymer undergoes thermal degradation when thermal compression is applied to the polymer layer during wafer bonding. When a polymer thermally expands, mechanical stresses are simultaneously applied to the interface and the polymer itself, which can induce micro- and nanoscale voids at the bonding interface.[23] Moreover, Cu−polymer bonding has low compatibility with Cu CMP,[24] which is a key process in advanced 3D packaging. To comprehensively understand the Cu−Cu bonding interface, Cu CMP is one of the most critical processes in advanced 3D packaging to avoid defects and yield drop during the 3D heterogeneous integration. In the case of Cu−polymer bonding, planarization of the Cu interface should be concurrently implemented with Cu passivation to achieve wafer-scale 3D vertical scalability. Owing to the low

https://doi.org/10.1021/acsami.4c04665
ACS Appl. Mater. Interfaces XXXX, XXX, XXX−XXX

viscoelasticity[25] and adhesiveness of semicured polymers, reliable planarization and curing of the Cu surface are not possible with conventional polymers, in which multiple surface defects are induced owing to the low modulus of the polymers. To achieve high-quality Cu−polymer bonding interfaces, additional polymer coating processes are required for polymer epoxy films.[26] As the polymer epoxy films are nonconductive,[27] complete conduction between the Cu interconnects can be achieved only under specific temperature conditions. While the epoxy-based bonding involves placing a micrometer-scale thick epoxy film on a chip and pressing it down at high temperatures, the solder melting point must be carefully controlled to remove organic residues from the joint, followed by curing at the reflow temperature. Therefore, the epoxy insulation completely limits the conduction through the Cu bonding interfaces.[16]

To overcome the limitations of Cu−polymer bonding, we present a wafer-scale bonding method via NHC nanolayer passivation that affords ultrastable thermomechanical properties, low-temperature bonding, robust corrosion inhibition, enhanced electrical conductivity, and back-end-of-line process compatibility with fabrication process reduction. Previous studies have reported the formation of N-heterocyclic carbene (NHC) nanolayers[28] that exhibit ultrastable properties at high temperatures.[29−34] Specifically, NHC nanolayers have been shown to exhibit high crystallinity, packing density, and thermal stability.[35] Additionally, NHC nanolayers effectively inhibit metal corrosion by binding to metal surfaces and forming stable self-assembled nanolayers, owing to their excellent chemical stability.[36,37] Furthermore, NHC nanolayers exhibit conductive properties owing to the low charge density of the carbene atoms, which causes electron-pulling effects.[38] Based on analysis of the work function and electrical potential using Kelvin probe force microscopy (KPFM), charge transfer occurs through Cu−C bonds on the Cu surface. The reproducibility and reliability of the stable current characteristics in the Cu−NHC−Cu 3D vertical structure were verified by conductive atomic force microscopy (CAFM) current−voltage (I−V) measurements. Additionally, the Cu−NHC complex was also investigated by analyzing the force−distance (F−D) curve, and the relative thermomechanical properties of the NHC nanolayer were clarified, enabling compatibility with CMP. According to this comprehensive characterization of the NHC nanolayer, it can be clarified that the NHC nanolayer enables the 3D heterogeneous integration with low-temperature bonding, wafer-scale, robust corrosion inhibition, and enhanced conductivity. Owing to its enhanced thermomechanical stability, NHC Cu/polymer bonding offers effective fabrication process reduction, in which additional polymer coating, passivation, epoxy coating, and cleaning processes can be omitted.

2. RESULTS AND DISCUSSION

2.1. Ultrastable N-Heterocyclic Carbene Passivation Nanolayers on the Cu (111) Surface. After patterning the bottom Cu electrode on a 4 in. Si−SiO_2 wafer, NHC nanolayers were synthesized by electrochemical deposition, as shown in Figure 1A,C. To electrochemically synthesize 1,3-diisopropylimidazolium chloride, a type of N-heterocyclic carbene, a negative potential (−1.3 V vs Ag/Ag^+) was applied to induce water reduction by forming hydroxide ions. The chemisorption mechanism of the NHC self-assembly was evaluated by characterizing the NHC nanolayers using various chemical analysis methods. The polymer (Figure 1B) and nanolayer (Figure 1D) used for film deposition were analyzed by Fourier transform infrared (FT-IR) spectroscopy. The IR peak at 1560 cm^{-1} is related to the symmetric stretching vibration of the imidazolium ring. An additional peak was detected at 2130 cm^{-1}, which is consistent with the symmetric C═C stretching vibration. The attenuated total reflectance infrared spectrum of the imidazolium salt precursor showed a sharp peak at 3290 cm^{-1}, related to the C−H vibration. As shown in Figure 1E, the carbene groups in the NHCs acted as anchoring groups, forming ultrastable and robust Cu−C bonds. Moreover, the two nitrogen atoms in the NHCs exhibited π-electron-donating properties, further enhancing the interaction between the NHCs and the copper surface compared to aryl−metal interactions. To investigate this Cu−NHC interaction, the NHC nanolayers were chemically characterized using X-ray photoelectron spectroscopy (XPS), as shown in Figure 1F. The C 1s XPS profile was deconvoluted into three Gaussian peaks centered at 285, 285.4, and 284.7 eV, assigned to the Cu−C, C−N, and C−C bonds, respectively, confirming stable NHC self-assembly and electrochemical deposition. As Cu can be easily degraded within an oxygen environment, the oxidation rate correlatively increases within a temperature increase. Furthermore, Cu oxide exhibits high resistivity and low reliability in Cu direct bonding. To avoid the oxidation of Cu, passivation is most widely used for low-temperature bonding and Cu surface protection, including the self-assembled monolayer, corrosion inhibitor, metal, organic solderability preservatives, and electroless nickel immersion gold. Subsequent thermomechanical analysis of the NHC nanolayers and the benzotriazole (BTA) passivation layer, which is the most widely used Cu passivation layer,[39−41] showed thermal expansion and contraction with cyclic temperature variations. Under the bonding conditions, BTA exhibited a sharp TMA displacement gradient, whereas NHC was ultrastable and exhibited a gradual displacement gradient. Furthermore, heterogeneous TMA displacement was observed for BTA and NHC. As shown in Figure 1G, BTA exhibited coexisting heterogeneous TMA displacement with increasing temperature, and the sharp decrease in the TMA displacement of BTA at 75 °C promotes defect formation and warpage at the surface and at the bond interface. However, NHC exhibited stable thermal contraction with increasing temperature and a gradual TMA displacement gradient above 100 °C, indicating that NHC can be reliably bonded at high temperatures. Most polymers have an amorphous phase comprising a completely disordered arrangement of polymer units. However, as the temperature decreases, the volume of the amorphous polymer shrinks, with shape retention, and the polymer is structurally arranged into a crystalline form in a certain direction. Thermogravimetric analysis of NHC and BTA directly indicated glass transition and melting behaviors in the bonding temperature range. The glass transition temperature (T_g) and melting point (T_m) of BTA were determined to be 38.7 and 78.6 °C, respectively, whereas the T_g and T_m of NHC were not observed within the bonding temperature range, which effectively hinders the development of crystallinity and phase transition during the Cu−polymer bonding process (Figure S1, Supporting Information).

2.2. Thermomechanical Stability of N-Heterocyclic Carbene Nanolayers. To verify the thermomechanical stability of the NHC nanolayers at the temperature used in the bonding process, a cyclic thermal shock was applied, which

https://doi.org/10.1021/acsami.4c04665
ACS Appl. Mater. Interfaces XXXX, XXX, XXX−XXX

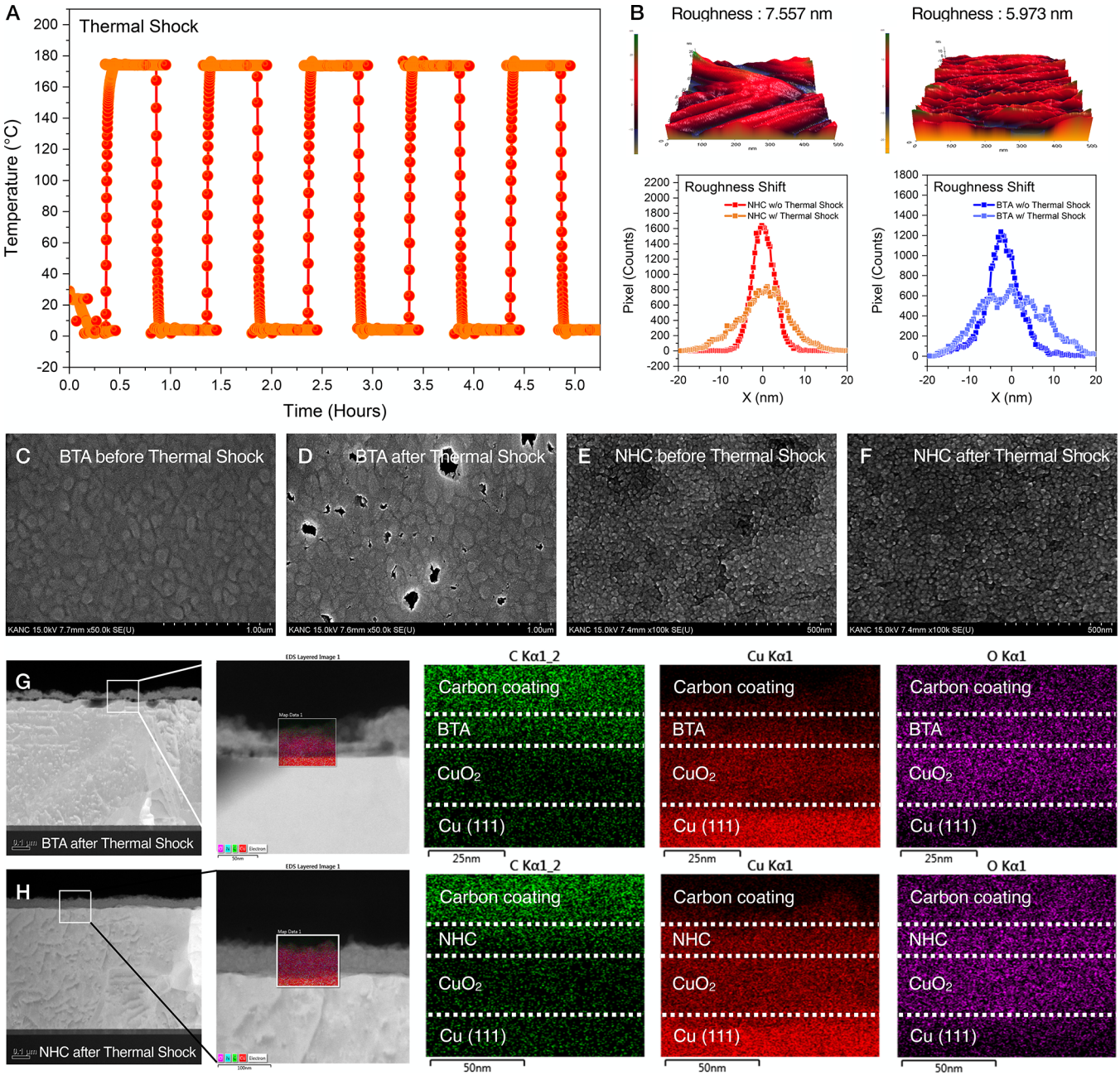

Figure 2. Verification of thermostability of organic passivation layers with cyclic thermal shock. (A) Time-dependent temperature variation during the cyclic thermal shock experiment at same temperature as bonding temperature (170 °C). (B) 3D topography and roughness pixel distribution of BTA passivation layer (left) and NHC passivation layer (right) after cyclic thermal shock. SEM observation of (C) BTA without thermal shock, (D) BTA with thermal shock, (E) NHC without thermal shock, and (f) NHC with thermal shock. Cross-sectional TEM-EDS observation of (G) BTA passivation layer and (H) NHC passivation layer after cyclic thermal shock, indicating microvoids at the bonding interfaces with BTA passivation layer, whereas NHC nanolayers exhibit ultrastable thermo-adhesive characteristics.

repeatedly rises and falls from 0 to 170 °C five times within 60 min intervals, as shown in Figure 2A. After the cyclic thermal shock, the NHC surface was spatially mapped based on the FD curve by probing each pixel (Figure 2B). The NHC roughness (5.973 nm) was smaller than the BTA roughness (7.557 nm), where the reduced roughness after the thermal shock is attributed to enhanced chemical bonding between the wingtip atoms of NHC during the annealing process, resulting in lateral polymerization. The surfaces of NHC and BTA were also compared after cyclic thermal shock at the same temperature as that used in the bonding process. The scanning electron microscopy (SEM) and transmission electron microscopy (TEM) images in Figure 2C–H show that in the case of BTA with low thermal stability, voids and defects appeared on the surface and at the interface of the passivation layer during the cyclic thermal shock (Figure S2). Compared with the BTA passivation layer, the NHC nanolayer exhibits ultrastable film quality with cyclic thermal shock. As shown in SEM and TEM characterization (Figure 2C–H), the NHC nanolayer does not indicate the remarkable degradation of film quality and crystallinity. According to the previous work about annealing effects of NHC nanolayer, annealing and thermal shock can

https://doi.org/10.1021/acsami.4c04665
ACS Appl. Mater. Interfaces XXXX, XXX, XXX−XXX

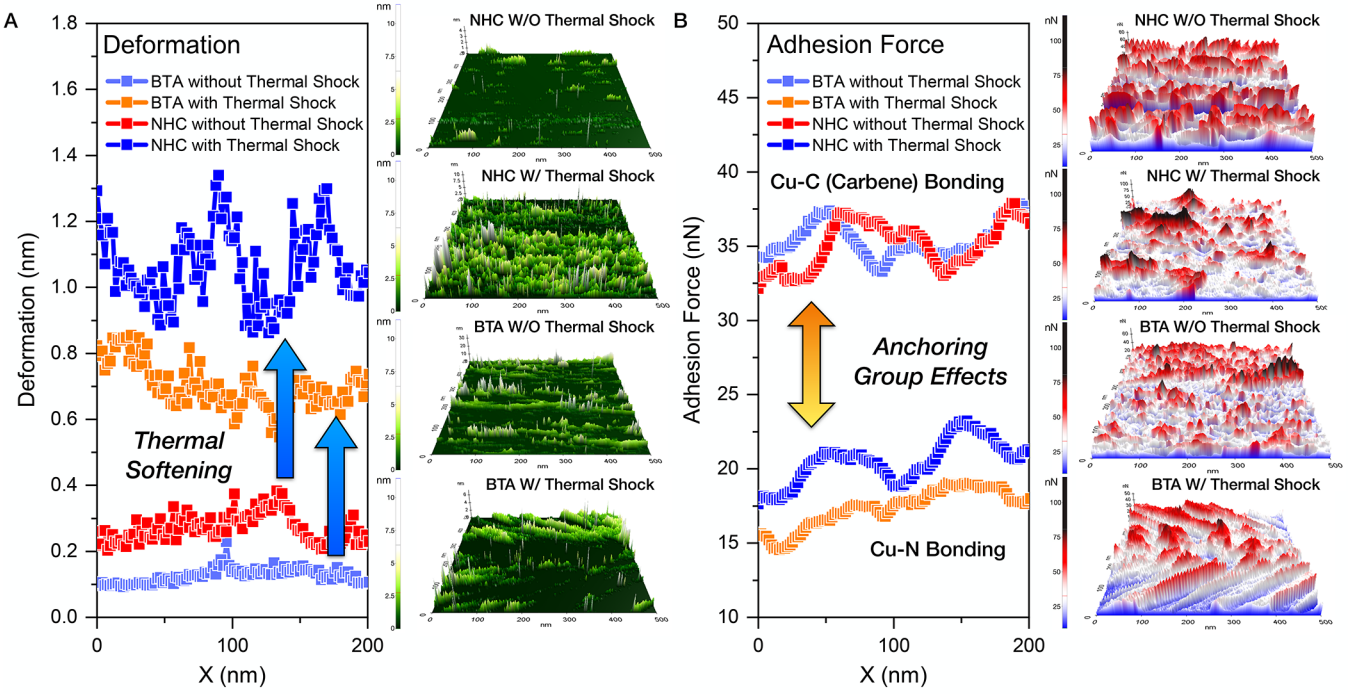

Figure 3. Spatial thermomechanical observation of Cu−polymer heterostructures with cyclic thermal shock. (A) Mechanical deformation and (B) adhesion force mapping of passivation layers via spatial FD curve mapping, which is significantly related to CMP compatibility and bonding strength. The mechanical deformation line profile after thermal shock indicates thermal softening effects, and the adhesion force line profile exhibits the robust chemical bonding strength of Cu−C bonding.

rather induce the removal of physisorbed residues[42] and enhanced crystallinity.[43] To further clarify the annealing effects of the NHC nanolayer, photoluminescence (PL) measurements have been conducted. Annealing of the NHC nanolayer effectively increases the crystallinity and its corresponding 6% enhanced photoresponsivity (Figure S3A). However, BTA passivation layer results in microvoids formation, which can be observed in top-view (SEM image) and cross-sectional view (TEM image). Additionally, AFM tip-induced nanoengineering was additionally conducted (Figure S3B). Nanoscale scratching clearly exhibits the corresponding mechanical deformation with spatial FD curve mapping results. Nonetheless, the NHC nanolayer exhibits a lower surface roughness compared to the BTA passivation layer, which is the most desirable surface condition for the Cu/polymer bonding process. Thus, the low mechanical strength of the NHC nanolayer can be compensated with robust corrosion inhibition, high surface quality, enhanced conductivity, and fabrication process shortening.

2.3. Highly Enhanced Crystallinity and Coverage of N-Heterocyclic Carbene Nanolayers. The highly enhanced crystallinity and coverage of the ultrastable NHC nanolayers based on Cu−C anchoring were confirmed through spatial FD curve mapping (Figure 3). As shown in Figure 3A, the NHC nanolayers were mechanically deformed by pressing with the AFM tip at a force of 450 nN. Under the influence of thermal shock, a thermal softening effect occurs in the organic layer, causing an increase in the overall deformation. The NHC nanolayers (0.387 nm without thermal shock and 1.043 nm with thermal shock) underwent greater mechanical deformation than the BTA layer (0.024 nm without thermal shock and 0.846 nm with thermal shock), which means that the NHC nanolayers are also compatible with Cu passivation and CMP processes. As shown in Figure 3B, when the AFM tip was pressed with a force of 450 nN and then released, the adhesion force of the NHC nanolayers (34.77 nN), which is the force required to detach the tip, was significantly (2.13-fold) higher than that of the BTA layer (16.31 nN), indicating that the Cu−C bond was significantly stronger than the Cu−N bond. The NHC domain expansion was verified by the structural self-assembly of NHC, which has lateral expandability. The NHC nanolayers were extended from the nanoscale domain to the microscale domain by annealing, as shown in Figure 2E,F. The higher degree of crystallinity observed in these NHC-iPr overlays is attributed to the iPr wingtip groups, which optimize the noncovalent effects in NHC, such as CH−π interactions. The reversible transition of upright and flat-lying species by annealing has been reported,[44] where heating an overlay of NHC-iPr above room temperature and annealing at 50 °C cause NHC-iPr to self-assemble into a zigzag arrangement, whereas heating at 75 °C converts some of the NHCs in the zigzag lattice to $(NHC)_2$−metal complexes, which then undergo a temperature-dependent structural transition to promote lateral polymerization and domain expansion. The annealing-induced crystallinity enhancement and structural transition of NHC nanolayers are highly advantageous in high-temperature and high-pressure environments. Expansion of the nanodomains in NHC resulted in a low defect density and excellent coverage, crystallinity, and packing density, which are significant in 3D heterogeneous integration environments.

2.4. Spatial Observation of Charge Transfer at the Cu−NHC Vertical Heterostructure. Previous studies have reported that the conductivity of NHC nanolayers is significantly enhanced through an electron-pulling effect, owing to the low electron density of the carbene atom. Because the conductivity of aromatic molecules at the metal−

https://doi.org/10.1021/acsami.4c04665
ACS Appl. Mater. Interfaces XXXX, XXX, XXX−XXX

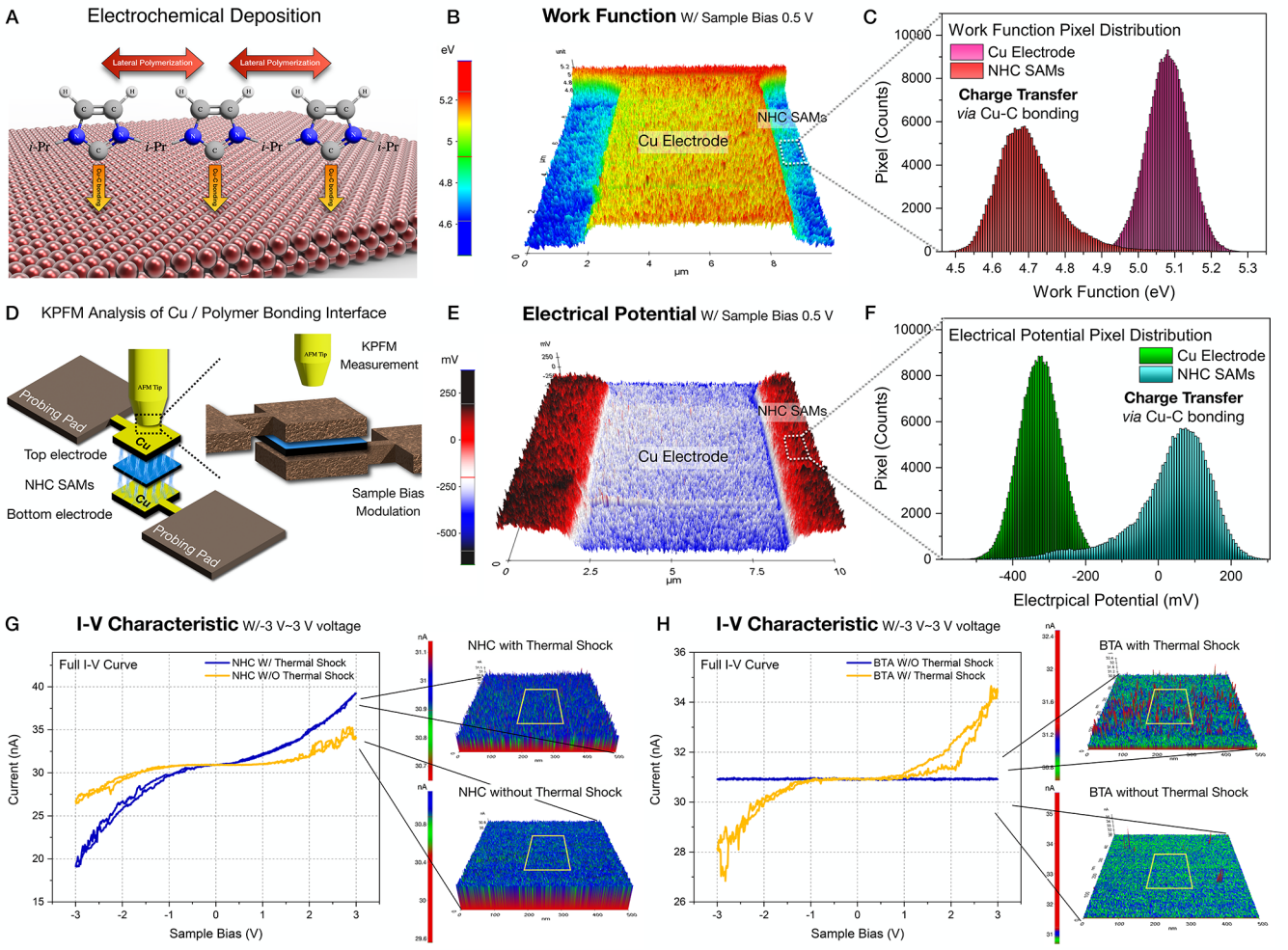

Figure 4. Microscopic analysis of NHC adsorption-induced electrical characteristic in Cu−polymer heterostructures. (A) Schematic of NHC self-assembly on Cu (111) surface. (B) Spatial distribution and (C) pixel distribution of work function in Cu electrode and NHC nanolayers. (D) Schematic of charge transfer detection in Cu−polymer−Cu vertical heterostructure. (E) Spatial distribution and (F) pixel distribution of electrical potential in Cu electrode and NHC nanolayers. Spatial CAFM *I*−*V* curve mapping of (G) NHC layer and (H) BTA layer, showing thermal shock effects.

molecule interfaces is strongly dependent on the electron density of the anchoring groups, the heterogeneous conductive properties of the NHC and BTA passivation layers were spatially observed. As shown in Figure 4A, the NHC was anchored to Cu (111) and synthesized on a 4 in. wafer scale via lateral polymerization, resulting in a tip-induced vertical stacking device with Cu (111) as the bottom electrode and the conductive AFM tip as the top electrode. As shown in Figures 4B and 4D, when a 0.5 V bias was applied to the sample, the electrons at the copper electrode were transferred to the NHC nanolayers. Thus, the electrical potential of the NHC nanolayers increased to 447.2 mV, while the work function decreased to 0.447 eV, which confirmed effective intramolecular charge transfer via the Cu−C bond. Figures 4C and 4F exhibit the pixel distributions of the measured work functions and electrical potentials, respectively. KPFM analysis showed that the carbene-induced interfacial dipole was the dominant factor influencing the experimentally observed shift of the Cu (111) work function. The current and charge-transfer characteristics were investigated by positioning the tip over a vertically integrated 3D structure, as shown in Figure 4D. In the case of BTA, a Cu−N bond is formed with the Cu atom, whereas in the case of NHC, the significant charge transfer (approximately 0.35−0.40 e^-) from the unshared electron pair of the carbene atom leads to the formation of a Cu−C bond (σ-donation), and simultaneously, negligible π-back-donation leads to the transfer of the carbene atom to the vacant 4d orbital of the Cu atom, forming a Cu−C bond. The high-electron-density anchoring group induces an electron-pushing effect, pushing the electrons away from the metal−molecule interfaces, whereas the low-electron-density anchoring group facilitates the electron-pulling effect, pulling the electrons toward the molecules[45] (Figure S4A). The conductivity of these carbene groups enables highly efficient intramolecular charge transfer via the Cu−C bond. To investigate the electrical properties of the NHC nanolayer, a CAFM junction has been constructed as a Pt/Ir tip (top electrode), NHC nanolayer, and Cu (111) (bottom electrode) (Figure S4B). To further clarify the tip−sample junction interface, scanning tunneling microscopy (STM) has been applied to investigate the current−distance spectroscopy, which enables the tip−sample junction interface to be within local pressure and interface charging effects (Figure S4C,D). When the tip is in noncontact state within tip−sample distance

https://doi.org/10.1021/acsami.4c04665
ACS Appl. Mater. Interfaces XXXX, XXX, XXX−XXX

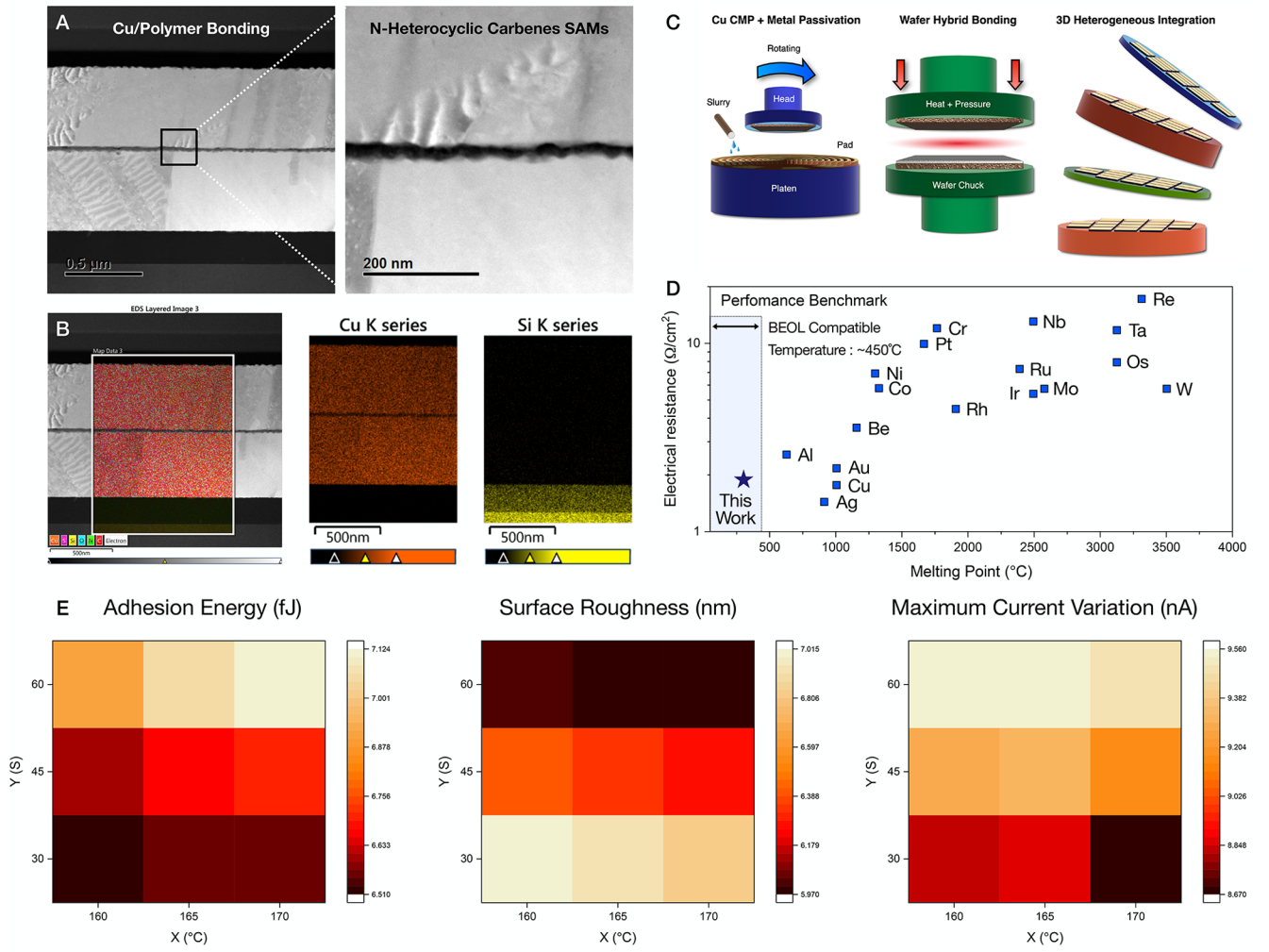

Figure 5. Wafer-scale 3D vertical-stacked heterostructure with NHC nanolayers. (A) TEM cross-sectional observation and (B) EDS mapping of Cu−polymer−Cu heterostructures, showing the formation of stable NHC nanolayers between Cu electrodes. (C) Schematic of fabrication of Cu/polymer bonding for 3D advanced packing, enabling efficient process reduction, with CMP compatibility, thermostability, and conductive characteristics. (D) Performance benchmark (electrical resistance and thermostability) of various metal passivation layers and NHC nanolayer, which exhibits ultralow electrical resistance and back-end-of-line compatible process temperature. (E) Heat map of performance benchmarks (adhesion energy, surface roughness, and maximum current variation) with temperature and process time.

variation, tunneling current was not observed in BTA, while maximum tunneling current was measured as 893.7 pA at the NHC. After the tip approach, interface charging between the tip and sample, current was amplified as nA scale. Moreover, current was gradually increased with tip-induced strain, which amplifies the interface charging and cross-sectional distance between top electrode (Pt/Ir tip) and bottom electrode (Cu wafer). Therefore, the current of NHC indicates the gradual increase as 40.12 nA with a tip−sample distance of −1.07 nm, while BTA exhibits the constant current as a 31.16 nA. Previous experiments[45] have reported that the conductivity of Cu−C bonds is higher than that of Cu−S bonds. The CAFM image pixel distribution indicates the existence of microvoids (31.2−31.5 nA) in BTA, whereas NHC only exhibited the 0.107 nA shift without microvoids (Figure S5). As shown in Figure 4G,H, BTA exhibited localized conduction properties, due to thermal degradation, whereas the current characteristics of NHC were unchanged upon cyclic thermal shock due to the stable thermomechanical properties, as the insulating properties were degraded and voids were created, exposing the Cu (111) surface.

2.5. Wafer-Scale 3D Heterogeneous Integration via N-Heterocyclic Carbene Nanolayers. Finally, the thermomechanical stability of the NHC nanolayers was verified by using a wafer-scale 3D vertical-stacking device structure. A Cu bottom electrode pattern (Figure S6) was fabricated by metal deposition on a 4 in. SiO_2 wafer. Electrochemical deposition of the NHC nanolayers resulted in site-selective passivation and coating only on the Cu electrode surface. Deposition area of NHC nanolayer was site-selectively designated in specific electrode area by previously reported fabrication process.[46] Cross-sectional transmission electron microscopy (TEM) images were acquired (Figure 5A) to correlate the thermomechanical stability of the fabricated Cu−NHC−Cu 3D vertically stacked structures. Based on the TEM observation, the obtained thickness of each layer was 517.46 nm for the Cu bottom electrode, 19.41 nm for the NHC nanolayers, and 542.29 nm for the Cu bottom electrode. Energy-dispersive spectroscopy (EDS) elemental mapping (Figure 5B) was performed to further clarify the construction of a stable 3D vertical structure with NHC nanolayers after cyclic thermal shock based on the elemental distribution of the

https://doi.org/10.1021/acsami.4c04665
ACS Appl. Mater. Interfaces XXXX, XXX, XXX−XXX

Cu and Si atoms. Figure 5C shows a schematic of the developed 3D heterogeneous integration process based on the NHC nanolayers, which consists of passivation, CMP, and Cu−polymer bonding. Cu CMP is the most significant process for Cu/polymer bonding because the planarized Cu surface, interface, and protrusions critically affect bonding. Nevertheless, polymer curing physically restrains slurry movement in the CMP pad, which hinders uniform surface planarization; thus, microscratches are generated in the unremoved central area.[16] Therefore, Cu CMP compatibility with ultrastable mechanical properties is highly desirable for preventing the formation of interfacial defects and voids in the 3D bonding structure. As mentioned earlier, the noble metal material has been recently implemented as Cu passivation to achieve reliable Cu−Cu bonding interfaces. As the key selection factor of metal for Cu passivation is electrical stability and thermomechanical stability, performance benchmark has been summarized with resistance and melting point of various noble metal materials (Figure 5D). Electrical resistivity of the NHC nanolayer was measured as 1.78×10^{-8} Ω·m, which is the 6% increased resistivity compared to the bulk Cu (111). Additionally, the melting point of NHC nanolayer has been measured as 270 °C, which can be compatible with back-end-of-line process temperature range. Comparing with these noble metal materials, the NHC nanolayer can concurrently take advantage of thermomechanical stability, warpage tolerance, and electrical conductivity. Finally, as performance benchmark parameters, the adhesion energy, surface roughness, and maximum current variation were analyzed to optimize the process conditions. Because annealing induces NHC domain expansion, the adhesion energy, surface roughness, and maximum current variation were linearly enhanced at higher temperatures and longer processing times. Above 170 °C and 1 min, stable bonding was also achieved with each 4 in. wafer, whereas stable bonding was not achieved below 170 °C and 1 min, attributed to insufficient domain expansion below the specific process conditions. Finally, the optimal conditions for the NHC Cu/polymer bonding process are 170 °C/1 min, which afforded the best performance factors in the fabrication of 3D vertical-stacked functional devices.

3. CONCLUSION

Wafer-scale bonding overcomes the physical limitations of conventional device downscaling and enables a 3D heterogeneous integration. Although the Cu−SiO_2 bonding technology is conventionally used, the demand for new bonding technologies is growing exponentially owing to the heterogeneous thermal expansion coefficient and weak bonding strength associated with Cu−SiO_2 bonding. Polymers have attracted significant attention as interfacial bonding materials because of their wide compatibility, high reliability, and high warpage tolerance. Because polymers exhibit extremely low thermomechanical stability, Cu−polymer bonding is limited to 3D packaging applications. Therefore, we presented the process of NHC Cu−polymer bonding, which enables ultrastable Cu−carbene chemical bonding, providing excellent thermal and chemical bonding strength even at a high temperature (170 °C). This resulted in high crystallinity and coverage with ultrastable thermomechanical properties, as observed by the roughness reduction and spatial FD curve mapping. Additionally, the low charge density of the carbene atom facilitated charge transfer through Cu−C bonding, allowing Cu−polymer bonding without removal of the NHC nanolayers and enabling effective process reduction. NHC Cu−polymer bonding structures are expected to advance the development of wafer-scale 3D chip architectures and functional integrated circuits.

4. EXPERIMENTAL SECTION

4.1. Deposition of N-Heterocyclic Carbene and Cu−Polymer Bonding. A 4 cm × 4 cm coupon wafer (Ti 500 Å/Cu 7000 Å) with Cu (111) was used in the experiments. The wafer was treated with HF and rinsed with isopropyl alcohol to remove the native oxide layer and organic contaminants. For NHC inhibition, 1,3- diisopropylimidazolium chloride was synthesized according to a previously published procedure. Electrochemical deposition was conducted using a metal-coated Si wafer as the working electrode, Ag/Ag^+ (CH Instruments) as the nonaqueous quasi-reference electrode, and a platinum wire as the counter electrode. A 50 mM solution of 1,3-diisopropylimidazolium chloride in acetonitrile, along with 0.1 M tetraethylammonium tetrafluoroborate (TEATFB), was used as the supporting electrolyte with 50 mM triply distilled water, at room temperature. NHC nanolayers were site-selectively deposited on the Cu (111) surface at a voltage of −1.3 V vs Ag/Ag^+ with 50 μs pulses for 5 min. Following pulsed electrochemical deposition, the sample was copiously rinsed with water and acetonitrile and dried under nitrogen. To fabricate the BTA passivation layer on Cu (111), the bare copper wafer was then immersed in an etchant solution for 1 min. The etchant solution consisted of deionized water (483.4 g), the complex agent [glycine] (5 g), pH adjuster [HNO_3] (0.1 mL), oxidant [H_2O_2] (16.67 g), and inhibitor [$C_6H_5N_3$] (0.25 g). During etching, the self-assembly proceeded concurrently to generate the BTA passivation layer directly on the Cu (111) surface. Cu−polymer bonding (wafer bonder; SB8GEN2, Süss MicroTec, Germany) was performed under the following thermocompression conditions: bonding temperature: 170 °C; bonding time: 1 min; vacuum: 1 mbar; force: 2100 N.

4.2. XPS Measurements and Data Analysis. XPS measurements (NEXSA, ThermoFisher Scientific, USA) were performed using an X-ray spot size of 400 μm. Peak analyses were conducted on the C 1s spectra. The XPS profiles were aligned by correcting the C 1s peak to a binding energy of 285 eV. After the measurements, the data were calibrated by using CASAXPS software (version 8.1).

4.3. AFM Measurements. KPFM, CAFM, and STM (AFM; NX-10, Park Systems, Republic of Korea) were performed using an ElectriMulti75-G cantilever. The KPFM reference work function was set to that of the highly oriented pyrolytic graphite sample (4.76 eV). CAFM spectroscopy was measured in the −3 to 3 V range within 50 nN for the contact state. Additionally, STM was conducted in room-temperature STM with ambient conditions for current−distance spectroscopy. The STM tip was fabricated via chemical etching of Au wire. The reference tunneling current was set with a highly oriented pyrolytic graphite (HOPG) sample. Reference tunneling current of HOPG was set as 0.37 pA and a 15 Å tip−sample distance. Current−distance spectroscopy was conducted with a scan rate of 0.4 Hz and 0.37 pA tunneling current. The FD curve (AFM; NX-10, Park Systems, Republic of Korea) was obtained by using an NM-RC-SEM cantilever. Thermal tuning tip calibration for the spring constant (347 N/m) and resonance frequency (776 Hz) was performed prior to acquiring the FD curve. Spatial FD curve mapping was conducted in contact mode, measuring 512 × 512 pixels at a size of 3 × 3 μm^2. The scan rate was set to 0.14 Hz, and the set point was 0.4 μm. The experimental FD curves were fitted theoretically by using the Hertzian contact model.

■ ASSOCIATED CONTENT

Supporting Information

The Supporting Information is available free of charge at https://pubs.acs.org/doi/10.1021/acsami.4c04665.

Figure S1: thermogravimetric analysis of (A) Cu−NHC complex and (B) Cu−BTA complex; Figure S2: HR-

https://doi.org/10.1021/acsami.4c04665
ACS Appl. Mater. Interfaces XXXX, XXX, XXX−XXX

TEM image of (A)−(D) BTA with thermal shock and (E)−(H) NHC with thermal shock; Figure S3: PL response with annealing and nanoscale scratches; Figure S4: (A) charge transfer dynamics, (B) CAFM junction, and (C), (D) *I*−*D* spectroscopy; Figure S5: CAFM current pixel distribution of (A), (B) BTA and (C), (D) NHC; Figure S6: OM image of fabricated Cu electrode patterns (PDF)

AUTHOR INFORMATION

Corresponding Author

Taesung Kim − *School of Mechanical Engineering, Sungkyunkwan University (SKKU), Suwon-si, Gyeonggi-do 16419, Republic of Korea; SKKU Advanced Institute of Nanotechnology (SAINT) and Department of Nano Science and Technology, Sungkyunkwan University, Suwon-si, Gyeonggi-do 16419, Republic of Korea; Department of Semiconductor Convergence Engineering, Suwon-si, Gyeonggi-do 16419, Republic of Korea; Department of Nano Engineering, Sungkyunkwan University, Suwon-si, Gyeonggi-do 16419, Republic of Korea;* orcid.org/0000-0001-6280-7668; Email: tkim@skku.edu

Authors

Jinhyoung Lee − *School of Mechanical Engineering, Sungkyunkwan University (SKKU), Suwon-si, Gyeonggi-do 16419, Republic of Korea; Center for Quantum Nanoscience, Institute for Basic Science (IBS), Seoul 03760, Republic of Korea*

Gunhoo Woo − *SKKU Advanced Institute of Nanotechnology (SAINT) and Department of Nano Science and Technology, Sungkyunkwan University, Suwon-si, Gyeonggi-do 16419, Republic of Korea*

Gyuyoung Lee − *School of Mechanical Engineering, Sungkyunkwan University (SKKU), Suwon-si, Gyeonggi-do 16419, Republic of Korea*

Jongyeong Jeon − *School of Mechanical Engineering, Sungkyunkwan University (SKKU), Suwon-si, Gyeonggi-do 16419, Republic of Korea*

Seunghwan Lee − *School of Mechanical Engineering, Sungkyunkwan University (SKKU), Suwon-si, Gyeonggi-do 16419, Republic of Korea*

Ziyang Wang − *School of Mechanical Engineering, Sungkyunkwan University (SKKU), Suwon-si, Gyeonggi-do 16419, Republic of Korea*

Hyelim Shin − *Department of Semiconductor Convergence Engineering, Suwon-si, Gyeonggi-do 16419, Republic of Korea*

Gil-Woo Lee − *School of Mechanical Engineering, Sungkyunkwan University (SKKU), Suwon-si, Gyeonggi-do 16419, Republic of Korea; Department of Physics, Konkuk University, Seoul 05029, Republic of Korea*

Yeon-Ji Kim − *School of Mechanical Engineering, Sungkyunkwan University (SKKU), Suwon-si, Gyeonggi-do 16419, Republic of Korea; Department of Physics, Konkuk University, Seoul 05029, Republic of Korea*

Do-Hyun Lee − *School of Mechanical Engineering, Sungkyunkwan University (SKKU), Suwon-si, Gyeonggi-do 16419, Republic of Korea; Department of Physics, Konkuk University, Seoul 05029, Republic of Korea*

Min-Jae Kim − *SKKU Advanced Institute of Nanotechnology (SAINT) and Department of Nano Science and Technology, Sungkyunkwan University, Suwon-si, Gyeonggi-do 16419, Republic of Korea*

Eungchul Kim − *AVP Process Development Team, Samsung Electronics, Chungcheongnam-do, Cheonan-si 31086, South Korea*

Hyunho Seok − *SKKU Advanced Institute of Nanotechnology (SAINT) and Department of Nano Science and Technology, Sungkyunkwan University, Suwon-si, Gyeonggi-do 16419, Republic of Korea;* orcid.org/0000-0002-3189-5930

Jinill Cho − *School of Mechanical Engineering, Sungkyunkwan University (SKKU), Suwon-si, Gyeonggi-do 16419, Republic of Korea*

Boseok Kang − *SKKU Advanced Institute of Nanotechnology (SAINT) and Department of Nano Science and Technology, Sungkyunkwan University, Suwon-si, Gyeonggi-do 16419, Republic of Korea; Department of Nano Engineering, Sungkyunkwan University, Suwon-si, Gyeonggi-do 16419, Republic of Korea;* orcid.org/0000-0003-4295-3881

You-Shin No − *Department of Physics, Konkuk University, Seoul 05029, Republic of Korea;* orcid.org/0000-0001-8947-4189

Won-Jun Jang − *Center for Quantum Nanoscience, Institute for Basic Science (IBS), Seoul 03760, Republic of Korea; Department of Physics, Ewha Womans University, Seoul 03760, Republic of Korea*

Complete contact information is available at: https://pubs.acs.org/10.1021/acsami.4c04665

Author Contributions

J.L., G.W., and G.L. contributed equally to this work. The manuscript was written through contributions of all authors. All authors have given approval to the final version of the manuscript. J.L., G.W., and G.L. prepared the samples and performed the main AFM experiments. J.J. and S.L. conducted TEM, EDS, XPS, XRD, and SEM measurements of NHC nanolayers. H.S. and Z.W. performed the NHC electrochemical deposition and device fabrication. G.-W.L., Y.K., and D.L. performed photoluminescence measurements of NHC nanolayers. M.K., E.K., H.S., and J.C. were involved in the technical discussions about mechanical properties of the NHC nanolayer. M.K., E.K., H.S., and Z.W. conducted the analytical experiments, including the TEM, EDS, XPS, XRD, and SEM measurements. B.K., Y.N., and W.J. technically discussed the structural properties of NHC nanolayers with J.L. J.L., G.W., and G.L. analyzed and discussed the experimental results. J.L. wrote the manuscript with contributions from all authors. T.K. designed and supervised the study.

Funding

This research was supported by the Basic Science Research Program of the National Research Foundation of Korea (NRF), funded by the Ministry of Education (No. 2022R1A3B1078163). This work was supported by the Institute for Basic Science (IBS-R027-D1). This research was supported by the MOTIE (Ministry of Trade, Industry & Energy (1415180243) and KSRC (Korea Semiconductor Research Consortium) (20020410) support program for the Development of Future Semiconductor Devices.

Notes

The authors declare no competing financial interest.

ABBREVIATIONS

NHC, N-heterocyclic carbene; MI, monolithic integration; HI, heterogeneous integration; CMP, chemical mechanical planarization; DBI, direct bond interface; CTE, coefficient of

thermal expansion; KPFM, Kelvin probe force microscopy; CAFM, conductive atomic force microscopy; *I*−*V*, current−voltage; FD, force−distance; BTA, benzotriazole; SEM, scanning electron microscopy; TEM, transmission electron microscopy; XPS, X-ray photoelectron spectroscopy; STM, scanning tunneling microscopy; PL, photoluminescence; EDS, energy-dispersive spectroscopy; FT-IR, Fourier-transform infrared; TMA, thermomechanical analysis.

REFERENCES

(1) Levinson, H. J.; Brunner, T. A. Current challenges and opportunities for EUV lithography. In *International Conference on Extreme Ultraviolet Lithography 2018*, 2018; SPIE: Vol. *10809*, pp 5−11.

(2) Kong, W.; Kum, H.; Bae, S.-H.; Shim, J.; Kim, H.; Kong, L.; Meng, Y.; Wang, K.; Kim, C.; Kim, J. Path towards graphene commercialization from lab to market. *Nat. Nanotechnol.* **2019**, *14* (10), 927−938.

(3) Lau, J. H. Recent advances and trends in advanced packaging. *IEEE Transactions on Components, Packaging and Manufacturing Technology* **2022**, *12* (2), 228−252.

(4) Liang, D.; Wei, T.; Wang, J.; Li, J. Quasi van der Waals epitaxy nitride materials and devices on two dimension materials. *Nano Energy* **2020**, *69*, 104463.

(5) Liu, Y.; Huang, Y.; Duan, X. Van der Waals integration before and beyond two-dimensional materials. *Nature* **2019**, *567* (7748), 323−333.

(6) Kim, Y.; Cruz, S. S.; Lee, K.; Alawode, B. O.; Choi, C.; Song, Y.; Johnson, J. M.; Heidelberger, C.; Kong, W.; Choi, S.; et al. Remote epitaxy through graphene enables two-dimensional material-based layer transfer. *Nature* **2017**, *544* (7650), 340−343.

(7) Chang, C. S.; Kim, K. S.; Park, B.-I.; Choi, J.; Kim, H.; Jeong, J.; Barone, M.; Parker, N.; Lee, S.; Zhang, X.; et al. Remote epitaxial interaction through graphene. *Science Advances* **2023**, *9* (42), No. eadj5379.

(8) Kim, E.; Choi, S.; Jeon, S.; Seok, H.; Cho, J.-i.; Shin, D.; Kim, T. Development of novel multi-selective slurry with mechanically driven etching for through silicon via chemical mechanical polishing. *Materials Science in Semiconductor Processing* **2022**, *152*, 107025.

(9) Elsherbini, A.; Liff, S.; Swan, J.; Jun, K.; Tiagaraj, S.; Pasdast, G. Hybrid bonding interconnect for advanced heterogeneously integrated processors. In *2021 IEEE 71st Electronic Components and Technology Conference (ECTC)*, 2021; IEEE: pp 1014−1019.

(10) Kang, Q.; Wang, C.; Zhou, S.; Li, G.; Lu, T.; Tian, Y.; He, P. Low-temperature Co-hydroxylated Cu/SiO_2 hybrid bonding strategy for a memory-centric chip architecture. *ACS Appl. Mater. Interfaces* **2021**, *13* (32), 38866−38876.

(11) Li, G.; Kang, Q.; Niu, F.; Wang, C. Recent progress on bumpless Cu/SiO_2 hybrid bonding for 3D heterogeneous integration. *Microelectronics International* **2023**, *40* (2), 115−131.

(12) Oprins, H.; Cherman, V.; Webers, T.; Kim, S.-W.; de Vos, J.; Van der Plas, G.; Beyne, E. 3D wafer-to-wafer bonding thermal resistance comparison: Hybrid Cu/dielectric bonding versus dielectric via-last bonding. In *2020 19th IEEE Intersociety Conference on Thermal and Thermomechanical Phenomena in Electronic Systems (ITherm)*, 2020; IEEE: pp 219−228.

(13) Tsau, Y. W.; De Messemaeker, J.; Salahouelhadj, A.; Gonzalez, M.; Witters, L.; Zhang, B.; Seefeldt, M.; Beyne, E.; De Wolf, I. Simulation of Cu pad expansion in wafer-to-wafer Cu/SiCN hybrid bonding. *Microelectronics Reliability* **2022**, *138*, 114716.

(14) James, J.; Spittle, J.; Brown, S.; Evans, R. A review of measurement techniques for the thermal expansion coefficient of metals and alloys at elevated temperatures. *Measurement science and technology* **2001**, *12* (3), R1.

(15) Lee, C.-H.; Tan, C.-A.; Fowler, M.; Ko, T.-Y.; Lin, Y.-M.; Chiu, W.-L.; Lee, O.-H.; Chen, K.-N. Negative-Tone Photosensitive Polymeric Bonding Material to Enable Room Temperature Pre-Bond for Cu/Polymer Hybrid Bonding. *IEEE Transactions on Components, Packaging and Manufacturing Technology* **2023**, *13*, 1316.

(16) Park, J.; Kang, S.; Kim, M. E.; Kim, N. J.; Kim, J.; Kim, S.; Kim, K. M. Advanced Cu/Polymer Hybrid Bonding System for Fine-Pitch 3D Stacking Devices. *Advanced Materials Technologies* **2023**, *8*, 2202134.

(17) Ma, S.; Wang, Y.; Min, Z.; Zhong, L. Nano/Mesoporous Polymers Based Low-k Dielectric Materials: A Review on Methods and Advances. *Advances in polymer technology* **2013**, DOI: 10.1002/adv.21358.

(18) Hu, C.-K.; Luther, B.; Kaufman, F.; Hummel, J.; Uzoh, C.; Pearson, D. Copper interconnection integration and reliability. *Thin Solid Films* **1995**, *262* (1−2), 84−92.

(19) Hakimian, E.; Sulong, A. B. Analysis of warpage and shrinkage properties of injection-molded micro gears polymer composites using numerical simulations assisted by the Taguchi method. *Materials & Design* **2012**, *42*, 62−71.

(20) Chulikavit, N.; Huynh, T.; Khatibi, A.; Das, R.; Kandare, E. Thermal degradation and flame spread characteristics of epoxy polymer composites incorporating mycelium. *Sci. Rep.* **2023**, *13* (1), 17812.

(21) Sánchez-Jiménez, P. E.; Pérez-Maqueda, L. A.; Perejón, A.; Criado, J. M. Constant rate thermal analysis for thermal stability studies of polymers. *Polymer degradation and stability* **2011**, *96* (5), 974−981.

(22) Suga, T.; He, R.; Vakanas, G.; La Manna, A. Direct Cu to Cu bonding and alternative bonding techniques in 3D packaging. *3D Microelectronic Packaging: From Architectures to Applications* **2021**, *64*, 201−231.

(23) Zhang, X. X.; Raskin, J.-P. Low-temperature wafer bonding: a study of void formation and influence on bonding strength. *J. Microelectromech. Syst.* **2005**, *14* (2), 368−382.

(24) Aoki, M.; Hozawa, K.; Takeda, K. Wafer-level hybrid bonding technology with copper/polymer co-planarization. In *2010 IEEE International 3D Systems Integration Conference (3DIC)*, 2010; IEEE: pp 1−4.

(25) Plazek, D. J.; O'Rourke, V. M. Viscoelastic behavior of low molecular weight polystyrene. *Journal of Polymer Science Part A-2: Polymer Physics* **1971**, *9* (2), 209−243.

(26) Ko, C.-T.; Chen, K.-N.; Lo, W.-C.; Cheng, C.-A.; Huang, W.-C.; Hsiao, Z.-C.; Fu, H.-C.; Chen, Y.-H. Wafer-level 3D integration using hybrid bonding. In *2010 IEEE International 3D Systems Integration Conference (3DIC)*, 2010; IEEE: pp 1−4.

(27) Lu, C.-H.; Jhu, S.-Y.; Chen, C.-P.; Tsai, B.-L.; Chen, K.-N. Asymmetric wafer-level polyimide and Cu/Sn hybrid bonding for 3-D heterogeneous integration. *IEEE Trans. Electron Devices* **2019**, *66* (7), 3073−3079.

(28) Inayeh, A.; Groome, R. R.; Singh, I.; Veinot, A. J.; de Lima, F. C.; Miwa, R. H.; Crudden, C. M.; McLean, A. B. Self-assembly of N-heterocyclic carbenes on Au (111). *Nat. Commun.* **2021**, *12* (1), 4034.

(29) Bosse, F.; Gutheil, C.; Nguyen, D. T.; Freitag, M.; Das, M.; Tyler, B. J.; Adolphs, T.; Schafer, A. H.; Arlinghaus, H. F.; Glorius, F.; Ravoo, B. J. Selective Removal of Gold: N-Heterocyclic Carbenes as Positive Etch Resists on Planar Gold Surfaces. *ACS Appl. Mater. Interfaces* **2023**, *15* (30), 36831−36838.

(30) Chang, L.-M.; An, Y.-Y.; Li, Q.-H.; Gu, Z.-G.; Han, Y.-F.; Zhang, J. N-Heterocyclic carbene as a surface platform for assembly of homochiral metal-organic framework thin films in chiral sensing. *ACS Appl. Mater. Interfaces* **2020**, *12* (34), 38357−38364.

(31) Choi, Y.; Park, C. S.; Tran, H.-V.; Li, C.-H.; Crudden, C. M.; Lee, T. R. Functionalized N-Heterocyclic Carbene Monolayers on Gold for Surface-Initiated Polymerizations. *ACS Appl. Mater. Interfaces* **2022**, *14* (39), 44969−44980.

(32) Li, Z.; Munro, K.; Narouz, M. R.; Lau, A.; Hao, H.; Crudden, C. M.; Horton, J. H. Self-assembled N-heterocyclic carbene-based carboxymethylated dextran monolayers on gold as a tunable platform for designing affinity-capture biosensor surfaces. *ACS Appl. Mater. Interfaces* **2018**, *10* (21), 17560−17570.

https://doi.org/10.1021/acsami.4c04665
ACS Appl. Mater. Interfaces XXXX, XXX, XXX−XXX

(33) Li, Z.; Narouz, M. R.; Munro, K.; Hao, B.; Crudden, C. M.; Horton, J. H.; Hao, H. Carboxymethylated dextran-modified n-heterocyclic carbene self-assembled monolayers on gold for use in surface plasmon resonance biosensing. *ACS Appl. Mater. Interfaces* **2017**, *9* (45), 39223−39234.
(34) Pellitero, M. A.; Jensen, I. M.; Dominique, N. L.; Ekowo, L. C.; Camden, J. P.; Jenkins, D. M.; Arroyo-Currás, N. Stability of N-Heterocyclic Carbene Monolayers under Continuous Voltammetric Interrogation. *ACS Appl. Mater. Interfaces* **2023**, *15* (29), 35701−35709.
(35) Crudden, C. M.; Horton, J. H.; Ebralidze, I. I.; Zenkina, O. V.; McLean, A. B.; Drevniok, B.; She, Z.; Kraatz, H.-B.; Mosey, N. J.; Seki, T.; et al. Ultra stable self-assembled monolayers of N-heterocyclic carbenes on gold. *Nat. Chem.* **2014**, *6* (5), 409−414.
(36) Trose, M.; Nahra, F.; Cazin, C. S. Dinuclear N-heterocyclic carbene copper (I) complexes. *Coord. Chem. Rev.* **2018**, *355*, 380−403.
(37) Wyer, E.; Gucciardo, G.; Leigh, V.; Müller-Bunz, H.; Albrecht, M. Comparison of carbene and imidazole bonding to a copper (I) center. *J. Organomet. Chem.* **2011**, *696* (17), 2882−2885.
(38) Krzykawska, A.; Wróbel, M.; Kozieł, K.; Cyganik, P. N-heterocyclic carbenes for the self-assembly of thin and highly insulating monolayers with high quality and stability. *ACS Nano* **2020**, *14* (5), 6043−6057.
(39) Grillo, F.; Tee, D. W.; Francis, S. M.; Früchtl, H. A.; Richardson, N. V. Passivation of copper: Benzotriazole films on Cu (111). *J. Phys. Chem. C* **2014**, *118* (16), 8667−8675.
(40) Li, J.; Lu, X. C.; Zhang, Z. B. Inhibition mechanism of benzotriazole in copper chemical mechanical planarization. *Applied Mechanics and materials* **2014**, *607*, 74−78.
(41) Wang, Q.; Tan, B.; Gao, B.; Tian, S.; Han, C.; Yang, L. Study on the adsorption and inhibition mechanism of 1, 2, 4-triazole on copper surface in copper interconnection CMP. *ECS Journal of Solid State Science and Technology* **2019**, *8* (6), P313.
(42) Berg, I.; Schio, L.; Reitz, J.; Molteni, E.; Lahav, L.; Bolanos, C. G.; Goldoni, A.; Grazioli, C.; Fratesi, G.; Hansmann, M. M.; Floreano, L.; Gross, E. Self-Assembled Monolayers of N-Heterocyclic Olefins on Au (111). *Angew. Chem., Int. Ed.* **2023**, *62* (46), No. e202311832.
(43) Berg, I.; Amit, E.; Hale, L.; Toste, F. D.; Gross, E. N-Heterocyclic Carbene Based Nanolayer for Copper Film Oxidation Mitigation. *Angew. Chem.* **2022**, *134* (25), No. e202201093.
(44) Ren, J.; Freitag, M.; Gao, Y.; Bellotti, P.; Das, M.; Schulze Lammers, B.; Monig, H.; Zhang, Y.; Daniliuc, C. G.; Du, S.; Fuchs, H.; Glorius, F. Reversible Self-Assembly of an N-Heterocyclic Carbene on Metal Surfaces. *Angew. Chem., Int. Ed.* **2022**, *61* (13), No. e202115104.
(45) Lee, J.; Kim, E.; Cho, J.; et al. Remote-Controllable Interfacial Electron Tunneling at Heterogeneous Molecular Junctions via Tip-Induced Optoelectrical Engineering. *Advanced Science* **2024**, *11* (5), 2305512.
(46) Amit, E.; Berg, I.; Zhang, W.; Mondal, R.; Shema, H.; Gutkin, V.; Kravchuk, T.; Toste, F. D.; Nairoukh, Z.; Gross, E. Selective Deposition of N-Heterocyclic Carbene Monolayers on Designated Au Microelectrodes within an Electrode Array. *Small* **2024**, *20* (2), 2302317.

https://doi.org/10.1021/acsami.4c04665
ACS Appl. Mater. Interfaces XXXX, XXX, XXX−XXX